

Multivariate continuous-time modeling of wind indexes and hedging of wind risk

April 14, 2020

Fred E. Benth¹, Troels S. Christensen^{2,3}, Victor Rohde⁴

Abstract

With the introduction of the exchange-traded German wind power futures, opportunities for German wind power producers to hedge their volumetric risk are present. We propose two continuous-time multivariate models for the wind power utilization at different wind sites, and discuss the properties and estimation procedures for the models. Employing the models to wind index data for wind sites in Germany and the underlying wind index of exchange-traded wind power futures contracts, the estimation results of both models suggest that they capture key statistical features of the data. We argue how these models can be used to find optimal hedging strategies using exchange-traded wind power futures for the owner of a portfolio of so-called tailor-made wind power futures. Both in-sample and out-of-sample hedging scenarios are considered, and, in both cases, significant variance reductions are achieved. Additionally, the risk premium of the German wind power futures is analysed, leading to an indication of the risk premium of tailor-made wind power futures.

JEL Classification: C3, G1, Q4.

Keywords: multivariate Ornstein-Uhlenbeck process; wind power futures; hedging; risk premium

1 Introduction

In the power market, producers in general face market risk in the sense of uncertainty of the prices at which they can sell their generated power. The intermittent nature of renewable energy sources such as wind and photo voltaic power production adds yet another layer of risk, known as volumetric risk in the sense that the produced amount of electricity is uncertain due to the dependence on weather. Globally, so-called power purchase agreements and subsidies from

¹Department of Mathematics, University of Oslo, PO Box 1053 Blindern, N-0316 Oslo, Norway

²Department of Mathematical Sciences, Aalborg University, Skjernvej 4A, 9220 Aalborg Øst, Denmark

³Quantitative Analytics, Centrica Energy Trading, Skelagervej 1, 9000 Aalborg, Denmark. Email address: troelsc@math.aau.dk (Troels S. Christensen)

⁴Department of Mathematics, Aarhus University, Ny Munkegade 118, 8000 Aarhus C, Denmark. Email address: victor@math.au.dk (Victor Rohde)

governments have minimized the market risk for renewable power producers. In contrast, the volumetric risk has only recently been addressed in Germany—and only for wind power producers (WPPs)—by the introduction of the exchange-traded wind power futures (WPF) contracts. The underlying of a WPF contract is an index between zero and one representing the overall utilization of the installed German wind power production. By taking an appropriate position in WPF contracts, the lost income of the WPPs implied by low wind scenarios is (partially) offset by the position in WPF contracts, hence minimizing the volumetric risk. Due to the prioritization of the cheapest power producers in Germany, the opposite part of the WPF market is typically conventional power producers (CPPs) such as gas-fired power plants. By taking an appropriate position in exchange-traded WPF contracts, CPPs can hedge their exposure to the cheap electricity generated by WPPs.

In consequence of the recent introduction of the WPF market, the related literature is limited. [10] consider the WPF market in great detail, and propose an equilibrium pricing model. They find that the willingness to engage in the WPF market is greater for the WPPs compared to CPPs. In other words, the hedging benefits of the WPF contracts are greater for WPPs than CPPs. This is supported by the results in [8] who employ an ARMA-GARCH copula framework to the joint modelling of one site-specific wind index and the underlying WPF index. In [6] modeling of the underlying WPF index is considered and closed-form formulas for the WPF price and the price of European options written on the WPF index are derived. A common feature of the mentioned articles is that they do not consider the simultaneous modeling of more than two wind indexes. Considering a portfolio of wind generation sites, where the production of electricity at each site is represented by the wind index at each wind site, a simultaneous model for the wind indexes at several wind sites is motivated for e.g. risk management of this portfolio. To the best of our knowledge, such simultaneous model is unexplored in the literature.

One way of constructing such simultaneous model is by using Lévy processes. Continuous-time modeling using univariate Ornstein-Uhlenbeck (OU) processes driven by non-decreasing Lévy processes, like the compound Poisson process with exponential jumps, have been studied extensively, and used to model, for example, stochastic volatility of financial assets, wind, electricity prices, and temperature (see [3, 4, 5, 6]). A detailed treatment of Lévy processes can be found in [15]. The multivariate modeling of more than two stochastic processes using multidimensional non-Gaussian Lévy processes is, however, more limited. Here we mention the work of [12] and [16] that introduce the multivariate construction by subordination of Brownian motions, and the work of [2] using linear transformations of Lévy processes.

Our contribution to the literature is twofold. Firstly, we propose a joint model for the simultaneous behaviour of wind indexes that allows for a parsimonious representation of the correlation structure. This model can be seen as the multivariate version of the model presented in [6]. As a consequence of the scarce literature on such multivariate models, we propose an alternative model for comparison reasons. Secondly, we suggest the idea of so-called tailor-made WPF contracts to eliminate the volumetric risk of WPPs completely. Employing our proposed joint model of wind indexes, we investigate the hedging benefits of exchange-traded WPF contracts for an owner of a portfolio of tailor-made WPF contracts, and comment on the risk premium of tailor-made WPF contracts. We

show that this construction is beneficial for both parties of the tailor-made WPF contracts.

The rest of the paper is organized as follows. Sec. 2 presents the data of wind indexes we later analyze in greater detail and also serves as motivation for the proposed model. In Sec. 3 we present models for the joint behaviour of wind indexes and corresponding estimation procedures. In Sec. 4 we present the estimation results of the two models. Sec. 5 discusses the hedging of wind power production using WPF contracts implied by the proposed models. Lastly, Sec. 6 concludes.

2 Data presentation

The empirical observation period spans from 1 July 2016 to 30 June 2019, which corresponds to 1095 daily observations for each considered wind index. The data set consists of

1. A daily wind index at three wind sites provided by Centrica Energy Trading. The wind index at wind site i is calculated by

$$\frac{Q_i(t)}{h(t)C_i},$$

where $h(t)$ is the number of hours in day t , $Q_i(t)$ is the power production at day t at site i , and C_i is the installed capacity at site i . Figure 1 shows the approximate geographical locations for the three wind sites.⁵

2. A daily German wind index provided by Nasdaq, representing the German utilization of wind power plants. The acronym used for it is NAREX WIDE (Nasdaq REnewable indeX WInd DE (Germany)) and is used as the underlying for WPF contracts traded on Nasdaq. We will simply denote it as the German wind index in the remaining part of the paper.

The wind indexes are bounded between zero and one. Fig. 2 shows all four wind indexes, and the corresponding autocorrelation function for each wind index. In all four cases, the wind index displays a pronounced yearly cycle consistent with the observations made in [6] and [8]. Since the German wind index is by construction made up of all wind power production in Germany, the behaviour of the German wind index is less extreme compared to the individual wind indexes. To concretize, a value of zero for the German wind index is not observed in our observation period, whereas it is for all three wind sites. Also the maximum attained value for each site wind index is higher than the maximum value of the German index; however, it does not reach one in any of the cases.

3 Model description

3.1 General model considerations

Let n denote the number of wind sites and $P_i(t)$ the i th wind index. We assume that the i th wind index can be described by

$$P_i(t) = 1 - e^{-S_i(t)X_i(t)}, \quad i = 1, \dots, n, \quad (3.1)$$

⁵The locations are approximate due to confidentially issues.

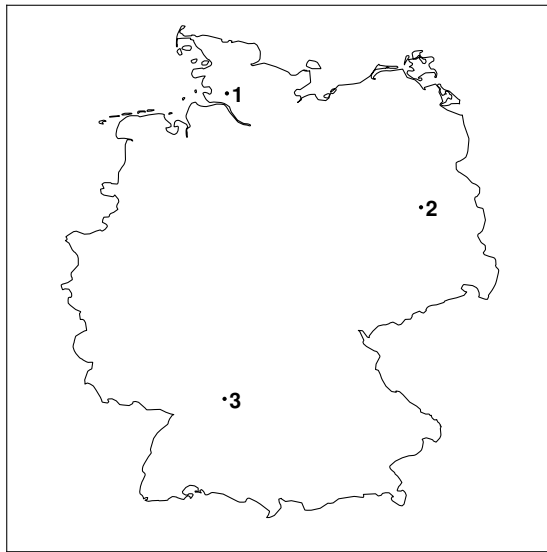


Figure 1: Locations of wind sites with site ID in Germany.

where $S_i(t) : \mathbb{R} \rightarrow \mathbb{R}^+$ is a deterministic function intended to filter out potential seasonal effects, and $X_i(t)$ is a mean-reverting stochastic process satisfying $X_i(t) \geq 0$ for all t . The intention of $X(t) = (X_1(t), \dots, X_n(t))^T$ is to capture the short-term uncertainty and the dependence between the n wind indexes. By this specification we are ensured that $P_i(t) \in [0, 1)$.

The proposed model in Eq. (3.1) distinguishes itself from the specification in [6], where the natural extension of their univariate setup to the present multivariate setup would be

$$P_i(t) = S_i(t)e^{-X_i(t)}. \quad (3.2)$$

with appropriate choices of $X_i(t)$ and $S_i(t)$. We do, however, prefer Eq. (3.1) over Eq. (3.2) for the following reasons. Firstly, due to our specification with regard to the deterministic part $S_i(t)$ of the model, we do not face any potential model inconsistencies as is the case of Eq. (3.2). We refer the interested reader to [6] for more information and discussion. Secondly, as discussed in Sec. 2, the wind index at a given site can attain a value of zero, whereas, on the other hand, we have not observed full utilization of the capacity at a single wind site. Since [6] consider the German wind index separately, which is never zero or one due to the construction of it, Eq. (3.2) is applicable without any modifications. Lastly, Eq. (3.1) implies that increased values of $S_i(t)$ and $X_i(t)$ translate to an increased value of $P_i(t)$, which is more intuitively appealing. In Eq. (3.2), increased values of $S_i(t)$ will still translate to increased values of $P_i(t)$, but here increased values of $X_i(t)$ translates to decreased values of $P_i(t)$.

Moving on to the seasonal components of the model, we include the following yearly seasonality motivated by the observations made in Fig. 2,

$$S_i(t) = a_i + b_i \sin(2\pi t/365) + c_i \cos(2\pi t/365), \quad i = 1, \dots, n,$$

where $a_i, b_i, c_i \in \mathbb{R}$. With N being the number of observations, the coefficients

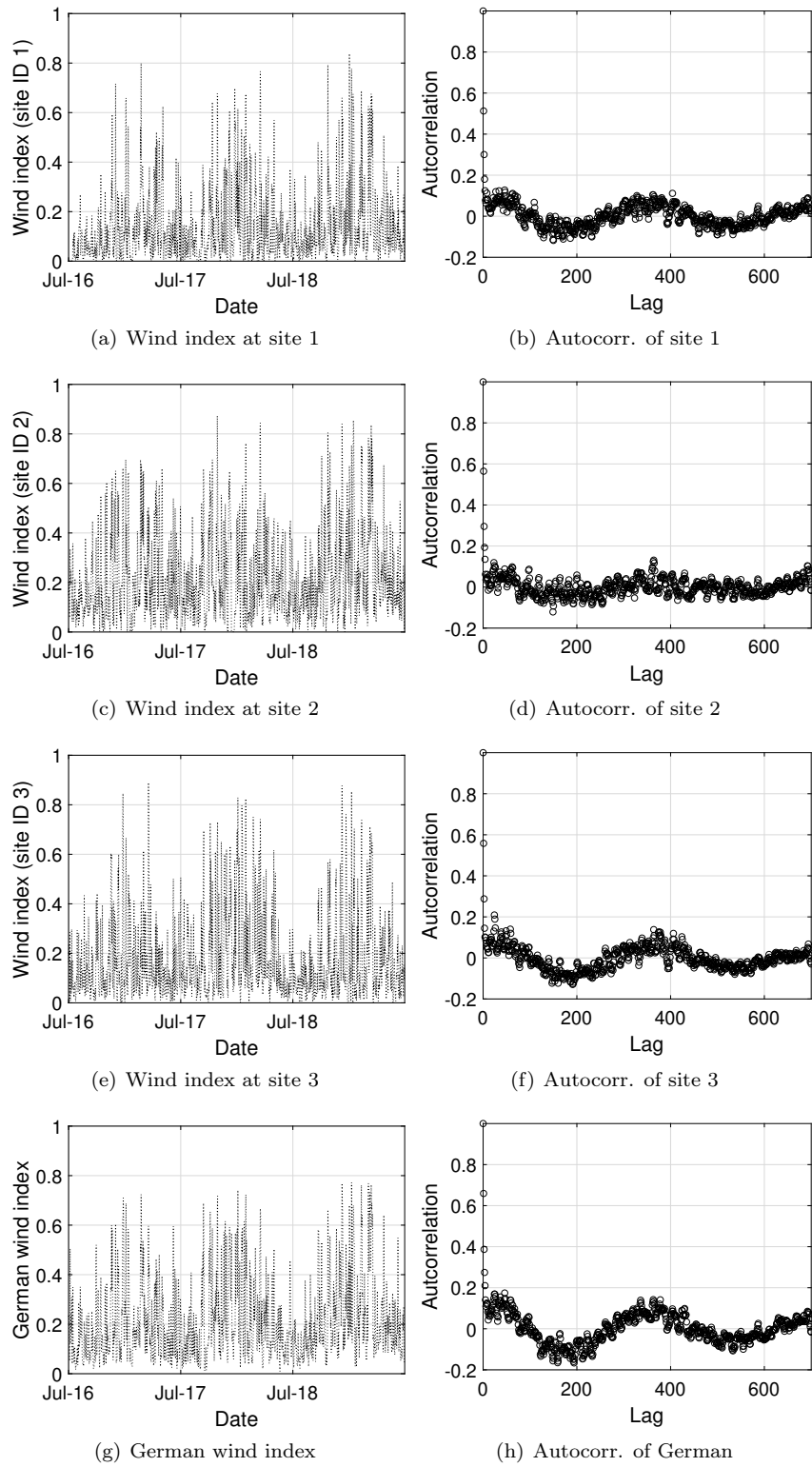


Figure 2: All four wind indexes with corresponding empirical auto-correlation function.

are determined by

$$\min_{a_i, b_i, c_i} \sum_{t=1}^N [-\log(1 - P_i(t)) - S_i(t)]^2, \quad i = 1, \dots, n.$$

Having obtained the estimated seasonal functions, the observed values of $X_i(t)$ implied by the estimated seasonal function $\hat{S}_i(t)$ can then be calculated as

$$X_i(t) = \frac{-\log(1 - P_i(t))}{\hat{S}_i(t)}. \quad (3.3)$$

We will in the following discuss two approaches for modeling $X_i(t)$.

3.2 A gamma model

In this section a multivariate model for $n - 1$ wind indexes and the German wind index is discussed, which we refer to as the gamma model in the sequel. In Sec. 4 we will consider the case $n = 4$. We start by introducing the noise process. In particular, we say a Lévy process L is a compound Poisson process with exponential jumps and parameters $\alpha > 0$ and $\beta > 0$ if

$$L(t) = \sum_{i=1}^{N(t)} J_i$$

where $(N(t))_{t \in \mathbb{R}}$ is a Poisson process with intensity α and J_i , $i \in \mathbb{N}$, are independent exponentially distributed random variables with parameter β . We say a random variable has an exponential distribution with parameter β if it has density $x \mapsto \mathbf{1}_{[0, \infty)}(x)\beta e^{-\beta x}$.

The gamma model assumes X is a multidimensional Lévy-driven Ornstein-Uhlenbeck (OU) process,

$$dX(t) = -\Lambda X(t)dt + \Sigma_L dL(t). \quad (3.4)$$

Here, L is an n -dimensional Lévy process where the i 'th entry is an independent compound Poisson process with exponential jumps, variance equal to one, and parameters α_i and β_i for $i = 1, \dots, n$. Furthermore, Λ is a diagonal matrix, $\text{diag}(\lambda_1, \dots, \lambda_n)$ with $\lambda_i > 0$ for $i = 1, \dots, n$. We assume Σ_L is given by

$$\Sigma_L = \begin{pmatrix} \sigma_{1,1} & 0 & \dots & 0 & \sigma_{1,n} \\ 0 & \sigma_{2,2} & \dots & 0 & \sigma_{2,n} \\ \vdots & \vdots & \ddots & 0 & \vdots \\ 0 & 0 & 0 & \sigma_{n-1,n-1} & \sigma_{n-1,n} \\ 0 & 0 & 0 & 0 & \sigma_{n,n} \end{pmatrix} \quad (3.5)$$

and that all entries of Σ_L are non-negative. Due to the form of Σ_L , each individual wind index has an idiosyncratic risk associated to it through one of the first $n - 1$ compound Poisson process L_1, \dots, L_{n-1} . Furthermore, all sites and the German index share a systematic risk through the n 'th compound Poisson process L_n . A similar construction is also considered in [2] where a multivariate model is proposed for modeling financial products written on more than one underlying asset.

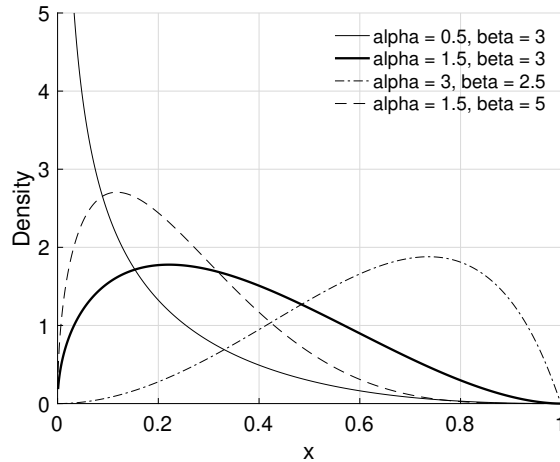


Figure 3: Different variations of the density in (3.6)

3.2.1 Distribution of $P_n(t)$ in the gamma model

The process associated with the German wind index, X_n , is an OU process driven by one compound Poisson process with exponential jumps, and it therefore has a gamma distribution as its stationary distribution. The processes X_1, \dots, X_{n-1} on the other hand are sums of two independent gamma distributions. The density of a sum of two independent gamma distributions does not, in general, have a closed form, and thus, there does not exist simple expressions for the densities of the individual site index similar to the one for the German index stated in Prop. 3.1.

Proposition 3.1. *The stationary distribution of $P_n(t)$ in the gamma model has density*

$$f_{P_n(t)}(x) = \frac{(-\log(1-x))^{\alpha_n-1} (1-x)^{\beta_n/S_n(t)-1}}{S_n(t)^{\alpha_n}} \quad x \in (0, 1) \quad (3.6)$$

Proof. This is a direct consequence of $X_n(t)$ being gamma distributed with shape α_n and rate β_n (see for example [3]). \square

In Figure 3 the density of P_n is depicted for different α_n and β_n (with $S_n(t) = 1$). We see that the densities implied by the gamma model are rather flexible and able to cover both low and high utilization scenarios.

3.2.2 Covariance between wind indexes in the gamma model

We now give (semi-)analytical expressions of the covariances implied by the gamma model, which will be useful for fast calculation of the minimum variance hedges discussed in Section 5.

Before we state the result, let us introduce some notation to help making a

concise statement. To this end define the $n \times (n+1)$ matrix $\tilde{\Sigma}_L$ by

$$\tilde{\Sigma}_L = \begin{pmatrix} \sigma_{1,1} & 0 & \dots & 0 & 0 & \sigma_{1,n} \\ 0 & \sigma_{2,2} & \dots & 0 & 0 & \sigma_{2,n} \\ \vdots & \vdots & \ddots & 0 & 0 & \vdots \\ 0 & 0 & 0 & \sigma_{n-1,n-1} & 0 & \sigma_{n-1,n} \\ 0 & 0 & 0 & 0 & 0 & \sigma_{n,n} \end{pmatrix}$$

where $\sigma_{i,j}$ is the (i,j) 'th entry of Σ_L . Let $\tilde{\sigma}_{i,j}$ denote the (i,j) 'th entry of $\tilde{\Sigma}_L$. Furthermore, define $\tilde{\alpha}, \tilde{\beta} \in \mathbb{R}^{n+1}$ by

$$\tilde{\alpha} = (\alpha_1, \dots, \alpha_{n-1}, 0, \alpha_n)^\top \quad \text{and} \quad \tilde{\beta} = (\beta_1, \dots, \beta_{n-1}, 1, \beta_n)^\top,$$

and denote the i 'th entry of $\tilde{\alpha}$ and $\tilde{\beta}$ by $\tilde{\alpha}_i$ and $\tilde{\beta}_i$. We now give the expressions of the covariances of the gamma model. The proof is relegated to the Appendix.

Proposition 3.2. *Consider $s \leq t$ and define*

$$f_{i,j}(u) = S_i(t)\tilde{\sigma}_{i,n+1}e^{-\lambda_i(t-s+u)} + S_j(s)\tilde{\sigma}_{j,n+1}e^{-\lambda_j u}, \quad i, j = 1, \dots, n.$$

Then

$$\begin{aligned} & \text{cov}(P_i(t), P_j(s)) \\ &= \left(\frac{\tilde{\beta}_i}{\tilde{\beta}_i + \tilde{\sigma}_{i,i}S_i(t)} \right)^{\tilde{\alpha}_i/\lambda_i} \left(\frac{\tilde{\beta}_{n+1} + \tilde{\sigma}_{i,n+1}S_i(t)e^{-\lambda_i(t-s)}}{\tilde{\beta}_{n+1} + \tilde{\sigma}_{i,n+1}S_i(t)} \right)^{\tilde{\alpha}_{n+1}/\lambda_i} \\ & \times \left(\frac{\tilde{\beta}_j}{\tilde{\beta}_j + \tilde{\sigma}_{j,j}S_j(s)} \right)^{\tilde{\alpha}_j/\lambda_j} \left[\left(1 + \frac{f_{i,j}(0)}{\tilde{\beta}_{n+1}} \right)^{\tilde{\alpha}_{n+1}f_{i,j}(0)/f'_{i,j}(0)} \right. \\ & \times \exp \left\{ \tilde{\alpha}_{n+1} \int_0^\infty \frac{d}{du} \left(\frac{f_{i,j}(u)}{\frac{d}{du}f_{i,j}(u)} \right) \log \left(1 + \frac{f_{i,j}(u)}{\tilde{\beta}_{n+1}} \right) du \right\} \\ & \left. - \left(\frac{\tilde{\beta}_{n+1}}{\tilde{\beta}_{n+1} + \tilde{\sigma}_{i,n+1}S_i(t)e^{-\lambda_i(t-s)}} \right)^{\tilde{\alpha}_{n+1}/\lambda_i} \left(\frac{\tilde{\beta}_{n+1}}{\tilde{\beta}_{n+1} + \tilde{\sigma}_{j,n+1}S_j(s)} \right)^{\tilde{\alpha}_{n+1}/\lambda_j} \right] \end{aligned} \quad (3.7)$$

for $i, j = 1, \dots, n$, $i \neq j$, and

$$\begin{aligned}
& \text{cov}(P_i(t), P_i(s)) \\
&= \left(\frac{\tilde{\beta}_i + \tilde{\sigma}_{i,i} S_i(t) e^{-\lambda_i(t-s)}}{\tilde{\beta}_i + \tilde{\sigma}_{i,i} S_i(t)} \right)^{\tilde{\alpha}_i/\lambda_i} \left(\frac{\tilde{\beta}_{n+1} + \tilde{\sigma}_{i,n+1} S_i(t) e^{-\lambda_i(t-s)}}{\tilde{\beta}_{n+1} + \tilde{\sigma}_{i,n+1} S_i(t)} \right)^{\tilde{\alpha}_{n+1}/\lambda_i} \\
&\times \left[\left(\frac{\tilde{\beta}_i}{\tilde{\beta}_i + (S_i(t) e^{-\lambda_i(t-s)} + S_i(s)) \tilde{\sigma}_{i,i}} \right)^{\tilde{\alpha}_i/\lambda_i} \right. \\
&\times \left(\frac{\tilde{\beta}_{n+1}}{\tilde{\beta}_{n+1} + (S_i(t) e^{-\lambda_i(t-s)} + S_i(s)) \tilde{\sigma}_{i,n+1}} \right)^{\tilde{\alpha}_{n+1}/\lambda_i} \\
&- \left(\frac{\tilde{\beta}_i^2}{(\tilde{\beta}_i + \tilde{\sigma}_{i,i} S_i(t) e^{-\lambda_i(t-s)}) (\tilde{\beta}_i + \tilde{\sigma}_{i,i} S_i(s))} \right)^{\tilde{\alpha}_i/\lambda_i} \\
&\times \left. \left(\frac{\tilde{\beta}_{n+1}^2}{(\tilde{\beta}_{n+1} + \tilde{\sigma}_{i,n+1} S_i(t) e^{-\lambda_i(t-s)}) (\tilde{\beta}_{n+1} + \tilde{\sigma}_{i,n+1} S_i(s))} \right)^{\tilde{\alpha}_{n+1}/\lambda_i} \right] \quad (3.8)
\end{aligned}$$

for $i = 1, \dots, n$.

The integral in Eq. (3.7) is the only non-analytical part of the expression, but we argue in Remark A.3 that this integral is small and can be coarsely approximated without significant effect. This allows us to maintain a fast computational speed when calculating the covariances. To further this point, we find a compute time, when evaluating (3.7) or (3.7) numerically 1,000 times, of around 0.03 seconds on a standard laptop implemented in MATLAB[®] R2018b.

3.2.3 Identification of parameters in the gamma model

Let Λ_{var} be the $n \times n$ matrix given by

$$(\Lambda_{var})_{i,j} = \frac{1}{\lambda_i + \lambda_j}.$$

Furthermore, denote by \circ the Hadamard product. Then the following result will be used to estimate the parameters of the gamma model. Again, we relegate the proof of Proposition 3.3 to the Appendix.

Proposition 3.3. *The mean of X is*

$$\mathbb{E}[X(0)] = \Lambda^{-1} \Sigma_L \beta / 2 \quad (3.9)$$

and the auto-covariance of X is

$$\text{cov}(X(0), X(t)) = (\Lambda_{var} \circ (\Sigma_L \Sigma_L^T)) e^{-\Lambda t} \quad (3.10)$$

for $t \geq 0$.

The parameters of the gamma model will be estimated in three steps. First, the mean-reversion matrix Λ will be fitted to the empirical auto-correlation function based on the first 25 lags. From (3.10), it follows that the model auto-correlation function of X_i is $t \mapsto e^{-\lambda_i t}$. To find $\hat{\lambda}_i$, the estimate of λ_i , we therefore minimize

$$\sum_{t=1}^{25} \left(\hat{\rho}_i(t) - e^{-\hat{\lambda}_i t} \right)^2$$

such that $\hat{\lambda}_i > 0$ for $i = 1, \dots, n$, where $\hat{\rho}_i(t)$ is the empirical auto-correlation function of X_i .

Next, $\hat{\Sigma}_L$ is chosen such that the model matches the empirical covariances. In particular, we choose $\hat{\Sigma}_L$ to minimize

$$\left\| \hat{\Sigma}_X - \Lambda_{var} \circ \left(\hat{\Sigma}_L \hat{\Sigma}_L^\top \right) \right\|^2$$

where $\hat{\Sigma}_X$ is the sample covariance of X , $\|\cdot\|$ is the Frobenius norm and the minimization is done over matrices $\hat{\Sigma}_L$ with non-negative entries of the form in (3.5).

Finally, we discuss how the parameters α and β are estimated. First, we choose $\hat{\beta} = (\hat{\beta}_1, \dots, \hat{\beta}_n)$ to minimize

$$\left\| \hat{\mu}_X - \Lambda^{-1} \hat{\Sigma}_L \hat{\beta} / 2 \right\|^2$$

such that $\hat{\beta}_i > 0$, where $\hat{\mu}_X$ is the empirical mean of X .

It is not too difficult to show that $\text{var}(L_i(1)) = 2\alpha_i/\beta_i^2$ and, since the compound Poisson processes are assumed to have unit variance, it therefore follows that

$$1 = \text{var}(L_i(1)) = \frac{2\alpha_i}{\beta_i^2}$$

Consequently, we take $\hat{\alpha}_i = \hat{\beta}_i^2/2$.

3.3 A lognormal model

In this section we present a lognormal model relying on different assumptions than the gamma model. We assume that $G(t) := \log X(t)$ can be modelled as a multidimensional Gaussian Ornstein-Uhlenbeck process,

$$dG(t) = -\Upsilon(G(t) - \Theta)dt + \Sigma dB(t), \quad (3.11)$$

where $(B(t))_{t \in \mathbb{R}}$ is an n -dimensional Brownian motion, $\Upsilon \in \mathbb{R}^{n \times n}$ is a diagonal matrix, $\Sigma \in \mathbb{R}^{n \times n}$ is a lower triangular matrix, and $\Theta \in \mathbb{R}^n$.

It is well-known (see e.g. [13]) that the stationary distribution of $G(t)$, when the diagonal elements of Υ all are positive, is normal with mean Θ . The autocovariance of $G(t)$ is given in, for example, [13], and it is the same as for the gamma model found in Prop. 3.3. In particular, we find

$$\Sigma_G(t) := \text{cov}(G(0), G(t)) = (\Upsilon_{var} \circ (\Sigma \Sigma^\top)) e^{-\Upsilon t}, \quad t \geq 0. \quad (3.12)$$

Here, Υ_{var} is the $n \times n$ matrix given by

$$(\Upsilon_{var})_{i,j} = \frac{1}{v_i + v_j},$$

where v_i is the i 'th entry of Υ , $i = 1, \dots, n$.

Consequently, the stationary distribution of $X(t)$ is multivariate lognormal with expected value of $X_i(0)$ being

$$\mathbb{E}[X_i(0)] = \exp\left(\Theta_i + \frac{\Sigma_G(0)_{ii}}{2}\right),$$

while the autocovariance is

$$\text{cov}(X_i(0), X_j(t)) = \mathbb{E}[X_i(0)]\mathbb{E}[X_j(0)](e^{\Sigma_G(t)_{ij}} - 1) \quad (3.13)$$

for $i, j = 1, \dots, n$ (see e.g. [11] for more information on the multivariate lognormal distribution). This implies that the autocorrelation of $X(t)$ is

$$\text{corr}(X_i(0), X_j(t)) = \frac{\exp(\Sigma_G(0)_{ij}e^{-tv_j}) - 1}{\sqrt{(e^{\Sigma_G(0)_{ii}} - 1)(e^{\Sigma_G(0)_{jj}} - 1)}}, \quad (3.14)$$

for $i, j = 1, \dots, n$.

3.3.1 Distribution of $P_i(t)$ in the lognormal model

Having the results for $X(t)$ from the previous section in mind, the stationary distribution of $P_i(t)$ is given in Prop. 3.4.

Proposition 3.4. *The stationary distribution of $P_i(t)$ is characterized by the density*

$$f_{P_i(t)}(x) = \frac{-1}{(1-x)\log(1-x)\sqrt{\Sigma_G(0)_{i,i}}}\phi\left(\frac{\log\left(-\frac{\log(1-x)}{S_i(t)}\right) - \Theta_i}{\sqrt{\Sigma_G(0)_{i,i}}}\right), \quad (3.15)$$

where $\Sigma_G(0)_{i,i}$ is the i 'th element of the diagonal of $\Sigma_G(0)$, Θ_i is the i 'th element of Θ , and $\phi(\cdot)$ is the density of the standard normal distribution.

To investigate the density of $P_i(t)$ in more detail, consider for a moment a more generic version of Eq. (3.15), given by

$$f(x|\mu, \sigma) = \frac{-1}{(1-x)\log(1-x)\sigma}\phi\left(\frac{\log(-\log(1-x)) - \mu}{\sigma}\right). \quad (3.16)$$

As can be seen in Fig. 4, showing examples of the density given different values of μ and σ in Eq. (3.16), the distribution is rather flexible and capable of attaining quite different forms.

3.3.2 Covariance between wind indexes in the lognormal model

Deriving the covariances between wind indexes in the lognormal model is closely related to the derivation of the Laplace transform of the lognormal distribution. To the best of our knowledge, no closed-form has been derived for the Laplace transform of the lognormal distribution, but there exist approximations, see e.g. [1]. With regard to this paper, we refer the interested reader to [1] and the references herein for further information, and employ numerical integration by exploiting our knowledge of the distribution of $G(t)$ to determine the covariances between the wind indexes.

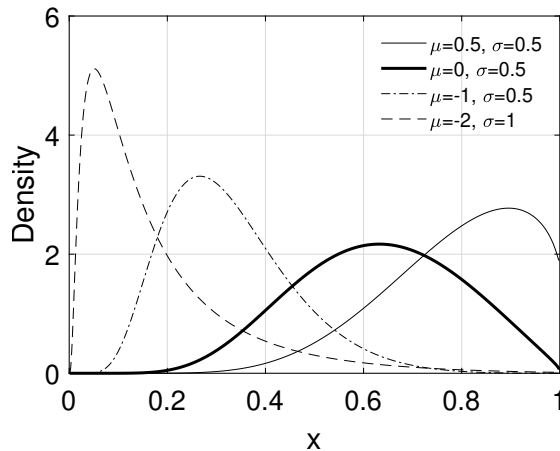


Figure 4: Different variations of the density in Eq. (3.16).

3.3.3 Identification of parameters in the lognormal model

To identify the parameters of the model, we employ the method of moments as in the gamma model case. We first identify $\Sigma_G(0)$ by exploiting Eq. (3.13),

$$\Sigma_G(0)_{ij} = \log \left(\frac{\hat{\Sigma}_{X,ij}}{\hat{\mu}_i \hat{\mu}_j} + 1 \right), \quad (3.17)$$

with $\hat{\mu}_i$ being the empirical mean of $X_i(t)$, and $\hat{\Sigma}_{X,ij}$ is the (i, j) th entry of the empirical covariance between $X_i(0)$ and $X_j(0)$.

Having obtained an estimate of $\Sigma_G(0)$ and remembering the model implied autocorrelation in Eq. (3.14), we identify v_i by minimizing

$$\sum_{t=1}^{25} \left(\hat{\rho}_i(t) - \frac{\exp \left(\hat{\Sigma}_G(0)_{ii} e^{-tv_i} \right) - 1}{\sqrt{(e^{\hat{\Sigma}_G(0)_{ii}} - 1)(e^{\hat{\Sigma}_G(0)_{ii}} - 1)}} \right)^2,$$

where $\hat{\rho}_i(t)$ is the empirical autocorrelation function of $X_i(0)$ and $X_i(t)$. Here, as in the gamma model, we use the first 25 lags of the empirical auto-covariance function to estimate λ_i . With $\hat{\Upsilon}$, consisting of the estimated v_i for $i = 1, \dots, n$ in the diagonal, at hand, we identify $\Sigma \Sigma^\top$ by

$$\Sigma \Sigma^\top = \hat{\Sigma}_G(0) \oslash \hat{\Upsilon}_{var},$$

where \oslash is the Hadamard division defined for two matrices A and B by $A \oslash B = A_{ij}/B_{ij}$. Lastly, we determine Θ by

$$\Theta_i = \log(\mu_i) - \frac{\hat{\Sigma}_G(0)_{ii}}{2}, \quad i = 1, \dots, n. \quad (3.18)$$

3.4 Comparison of the gamma and lognormal model

The covariances between indexes in the gamma model can be calculated fast using Proposition 3.2 to find the optimal hedging strategy (see Sec. 5). The noise

| | \hat{a}_i | \hat{b}_i | \hat{c}_i |
|--------|-------------|-------------|-------------|
| Site 1 | 0.1721 | -0.0491 | -0.0804 |
| Site 2 | 0.2848 | -0.0405 | -0.0956 |
| Site 3 | 0.2294 | -0.0322 | -0.1226 |
| German | 0.2732 | -0.0298 | -0.1285 |

Table 1: Fitted seasonal parameters for the four wind indexes.

in the gamma model also has a compelling interpretation, where an idiosyncratic risk is associated to each site index and a systematic risk is associated to all site indexes and the German index. On the other hand, the lognormal model gives rise to closed-form expressions of the densities of all indexes as opposed to only the German index in the gamma model. The lognormal model is simple in the sense that the underlying process is a Gaussian driven OU process. This makes it possible to do numerical analysis based on Gaussian theory.

Both the gamma and lognormal model have straightforward and fast estimation procedures, making them easy to implement. Furthermore, as we will see in Sec. 4, both models capture the autocorrelation of X_i , the cross-autocorrelations between X_i and X_j , and the stationary distribution of X_i well.

4 Estimation results

In this section we summarize and discuss the estimation results. As a starting point, we consider the fitted seasonal functions. In Table 1 we report the fitted parameters for all four wind indexes.

4.1 Gamma model

Fig. 5 shows the theoretical autocorrelation implied by the estimated gamma model compared to the empirical autocorrelation. The fit to the empirical autocorrelation is convincing, and it is worth noticing that the cross-autocorrelations match well even though the model has only been estimated to the marginal autocorrelation functions.

In Fig. 6 the histogram of X_i and the model density based on a simulation are shown. We see that the distribution of the wind sites implied by the gamma model have a convincing fit to the empirical distributions. The German wind index takes values close to zero more frequently than predicted by the gamma model, but besides this, the distribution of the gamma model gives a satisfying fit to the empirical distribution.

We report the estimated parameters in Table 2. The parameters α_4 and β_4 are considerably larger than α_i and β_i for $i = 1, 2, 3$. This implies that the systematic risk factor L_4 jumps much more frequently than L_i , $i = 1, 2, 3$, but that the jumps of L_4 are relatively small compared to the jumps of L_i , $i = 1, 2, 3$. This aligns well with the intuition that the systematic risk is associated to the wind utilization of the whole of Germany.

To further assess the model, we report in Table 3 the mean, variance, skewness, and kurtosis of the gamma model along with the empirical and lognormal

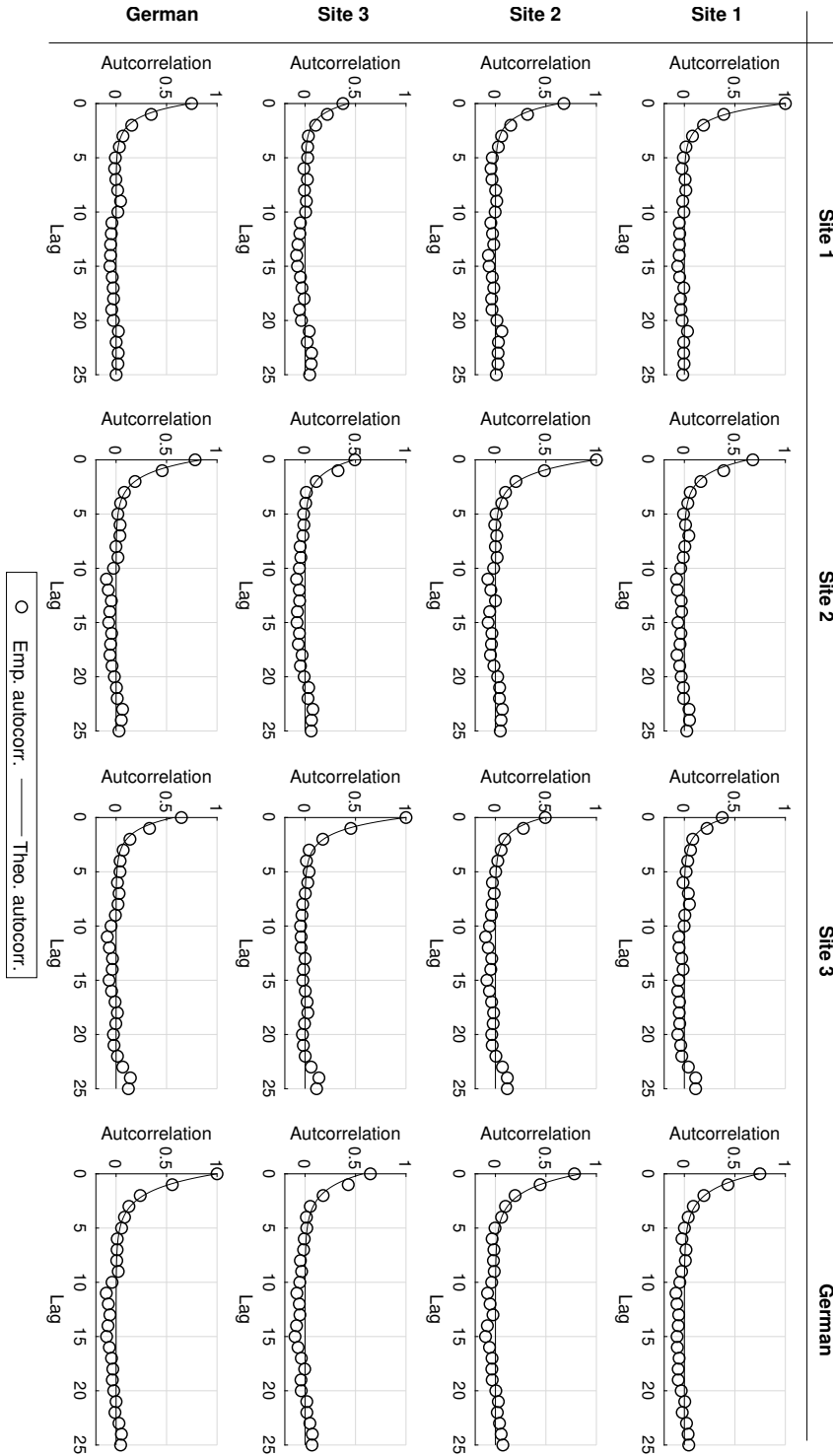


Figure 5: Empirical autocorrelation and theoretical autocorrelation implied by the fitted gamma model. The (i, j) 'th panel shows $\text{cor}(X_i(0), X_j(t))$ for $t = 0, 1, \dots, 25$.

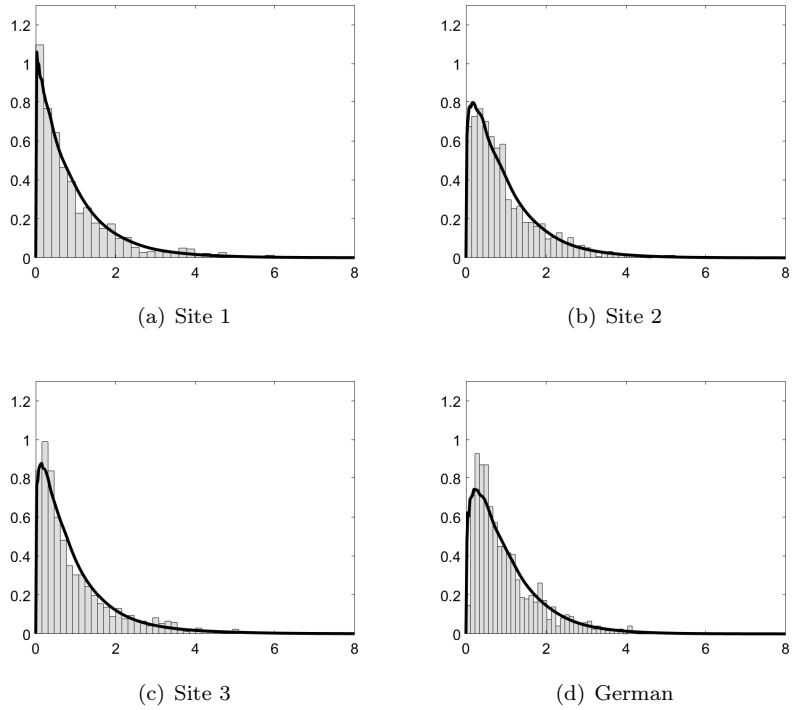


Figure 6: Histograms of $X_i(t)$ with the fitted densities of the gamma model.

| | $\hat{\alpha}_i$ | $\hat{\beta}_i$ | $\hat{\lambda}_i$ | $\hat{\sigma}_{i,i}$ | $\hat{\sigma}_{i,4}$ |
|--------|------------------|-----------------|-------------------|----------------------|----------------------|
| Site 1 | 0.0271 | 0.2328 | 0.8977 | 1.0305 | 1.1593 |
| Site 2 | 0.0538 | 0.3282 | 0.7589 | 0.6101 | 0.9792 |
| Site 3 | 0.1383 | 0.5260 | 0.8513 | 1.1674 | 0.8247 |
| German | 0.8960 | 1.3387 | 0.6539 | (-) | 0.9781 |

Table 2: Estimated parameters in the gamma model.

| | Mean | Variance | Skewness | Kurtosis |
|-----------|------|----------|----------|----------|
| Gamma | 1.00 | 0.73 | 1.71 | 7.38 |
| Lognormal | 1.00 | 0.73 | 3.17 | 24.98 |
| Empirical | 1.00 | 0.73 | 1.67 | 6.27 |

Table 3: Mean, variance, skewness, and kurtosis of the German wind index in the gamma and lognormal model together with the empirical values for the German wind index.

| | $\hat{\Theta}_i$ | \hat{v}_i |
|--------|------------------|-------------|
| Site 1 | -0.4282 | 0.7080 |
| Site 2 | -0.3215 | 0.6341 |
| Site 3 | -0.3803 | 0.6837 |
| German | -0.2711 | 0.5607 |

Table 4: Estimated parameters in the lognormal model.

equivalents for the German wind index⁶. The first two moment of the gamma model agrees with the empirical version as expected from the estimation procedure, where we match the gamma model to the empirical mean and variance. Further, the empirical skewness and kurtosis are captured within a reasonable precision by the gamma model.

4.2 Lognormal model

Fig. 7 shows the theoretical autocorrelation implied by the estimated lognormal model compared to the empirical autocorrelation. As in the gamma model case, the lognormal model captures the autocorrelation and cross-autocorrelation well, in particular taking into account that only the autocorrelation is used to estimate the parameters affecting both the autocorrelations and the cross-autocorrelations.

Fig. 8 shows histograms of the marginal distributions and the fitted lognormal densities. The lognormal model provides overall a decent fit, but seems to capture the distribution of the German wind index better than the site indexes. The estimated Θ and Υ for the lognormal model is reported in Table 4 and the estimated Σ is

$$\hat{\Sigma} = \begin{bmatrix} 1.0987 & 0 & 0 & 0 \\ 0.6763 & 0.5886 & 0 & 0 \\ 0.4902 & 0.3505 & 0.8376 & 0 \\ 0.6381 & 0.2539 & 0.2162 & 0.3035 \end{bmatrix}.$$

Although the speed of mean reversion parameters \hat{v}_i differ in the lognormal model compared to the gamma model, the same pattern is observed, with the German wind index being the most persistent.

Returning to Table 3, the lognormal model matches the empirical mean and variance as a results of the estimation procedure, but it does not capture the higher order standardized moments. This indicates that the lognormal model does not capture the whole distribution of the data as well as the gamma model.

⁶Since the same quantities for the site wind indexes are not relevant in the remaining part of the paper, we have chosen to omit them.

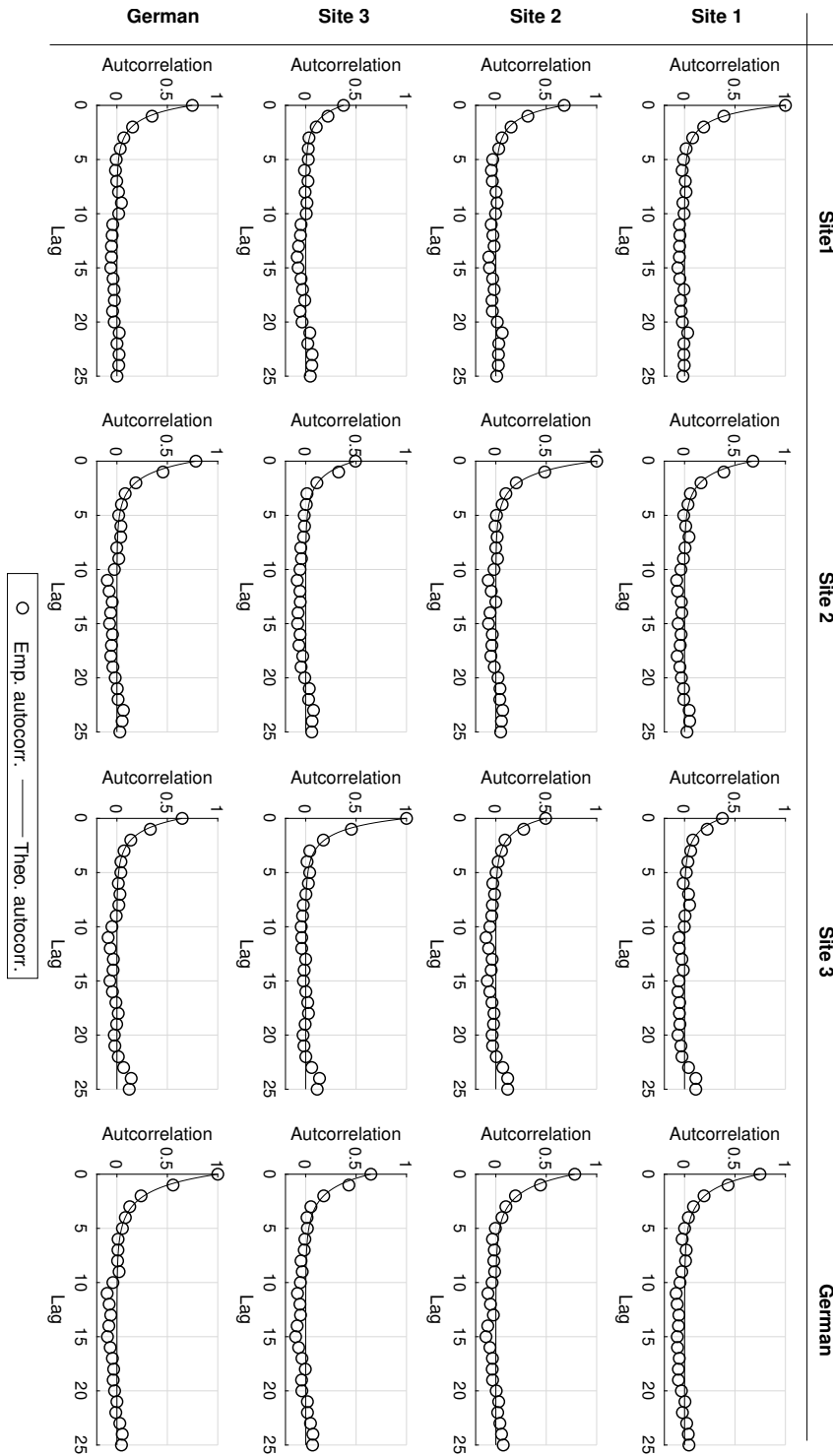


Figure 7: Empirical autocorrelation and theoretical autocorrelation implied by the fitted lognormal model. The (i, j) 'th panel shows $\text{cor}(X_i(0), X_j(t))$ for $t = 0, 1, \dots, 25$.

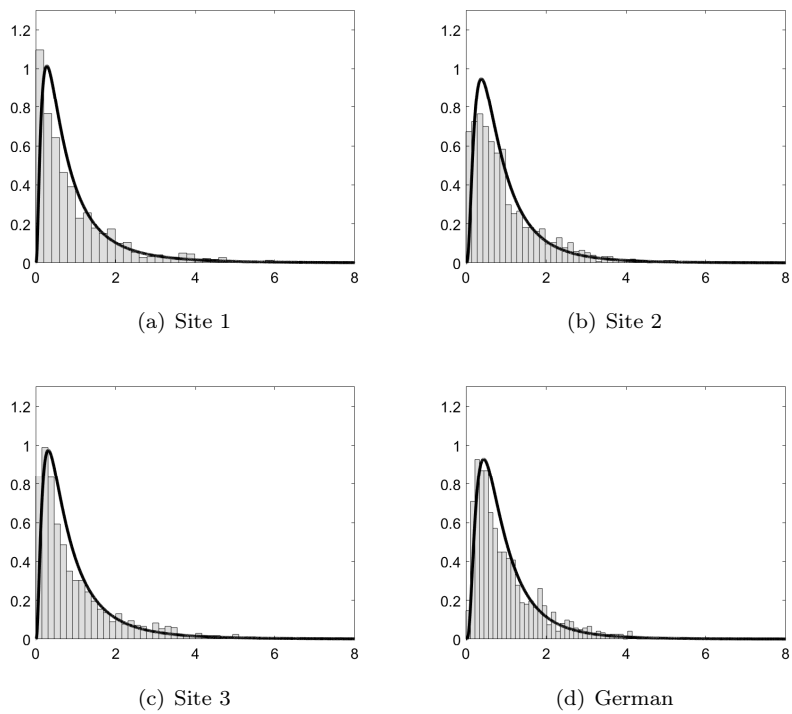


Figure 8: Histograms of $X_i(t)$ with fitted lognormal densities.

5 Hedging wind power production

In the following we denote the German wind index at day t by $P_n(t)$. An exchange-traded WPF contract is written on the underlying daily wind index, $P_n(t)$. The payoff of a long position in such a contract is

$$H(\bar{P}_n(S, T) - P_n(t_0, S, T))X, \quad (5.1)$$

where H is the number of hours during the delivery period $[S, T]$, $P_n(t_0, S, T)$ is the WPF price agreed on at time $t_0 < S < T$, X is a specified tick size, and

$$\bar{P}_n(S, T) = \frac{1}{T - S + 1} \sum_{t=S}^T P_n(t).$$

From Eq. (5.1) it is apparent that a short position results in a positive payoff in low wind scenarios according to the short position equivalent to Eq. (5.1),

$$H(P_n(t_0, S, T) - \bar{P}_n(S, T))X.$$

That is, if the realization of $\bar{P}_n(S, T)$ is lower than $P_n(t_0, S, T)$. This is favourable for a WPP, since this payoff will offset the loss in income from the long position in wind power production.

To be more specific, let C_i denote the capacity of WPP i , and let $P_i(t)$ denote the daily wind index/utilization of WPP i such that $C_i P_i(t)$ is the actual production of power. Further assume that the WPP receives a fixed price Q_i per produced MWh. The long position in wind power production for WPP i doing the period $[S, T]$ is therefore

$$\bar{P}_i(S, T)C_iHQ_i, \quad (5.2)$$

where

$$\bar{P}_i(S, T) = \frac{1}{T - S + 1} \sum_{t=S}^T P_i(t). \quad (5.3)$$

Assume that the WPP takes a position $\gamma_i \in \mathbb{Z}$ in WPF contracts with delivery period being $[S, T]$. The payoff from taking this position and the long position in wind power production results in a portfolio with payoff

$$H\bar{P}_i(S, T)C_iQ_i + \gamma_iH(\bar{P}_n(S, T) - P_n(t_0, S, T))X. \quad (5.4)$$

From Eq. (5.4) it is clear that perfectly hedging the volumetric risk would mean to choose γ_i such that $H\bar{P}_i(S, T)C_iQ_i = -\gamma_iH\bar{P}_n(S, T)X$, resulting in the deterministic payoff $\gamma_iHP_n(t_0, S, T)X$. However, the problem for the WPP is that the stochastic terms $\bar{P}_i(S, T)$ and $\bar{P}_n(S, T)$ are not perfectly dependent, and hence obtaining the deterministic payoff $\gamma_iHP_n(t_0, S, T)X$ is not possible. In fact, as shown in [8], it is far from optimal using the exchange-traded WPF contracts for hedging purposes for a single WPP, depending on the dependence structure between the site-specific wind index and the underlying index of the WPF contract.

5.1 Perfect hedging of volumetric risk using tailor-made wind power futures

Tailor-made over-the-counter WPF contracts is a way of perfectly hedging the volumetric risk. Instead of going short the exchange-traded WPF contract, the WPP could instead go short an over-the-counter WPF contract with the underlying being $P_i(t)$ instead of $P_n(t)$. In the following we therefore consider the situation of an energy management company (EMC) acting as counterparty of these tailor-made WPF contracts from $n-1$ different WPPs in Germany. Let $H(\bar{P}_i(S, T) - P_i(t_0, S, T))C_iQ_i$ be the payoff of a long position in a tailor-made WPF contract for WPP i . Thus, from the point of view of the EMC, the payoff of acting as counterparty for $n-1$ different WPPs and taking a position $\gamma \in \mathbb{Z}$ in the exchange-traded WPF contract is

$$R_C(\gamma) = \sum_{i=1}^{n-1} H(\bar{P}_i(S, T) - P_i(t_0, S, T))C_iQ_i + \gamma H(\bar{P}_n(S, T) - P_n(t_0, S, T))X, \quad (5.5)$$

while the payoff from the point of view of the i th WPP is

$$\begin{aligned} R_{WPP,i} &= H\bar{P}_i(S, T)C_iQ_i + H(P_i(t_0, S, T) - \bar{P}_i(S, T))C_iQ_i \\ &= HP_i(t_0, S, T)C_iQ_i. \end{aligned}$$

We argue that this construction can be beneficial for both the individual WPPs and the EMC: Firstly, the individual WPPs obtain a perfect hedge of their volumetric risk, and secondly, with an appropriate number of WPPs and distribution of the WPPs geographically, the portfolio of tailor-made WPF contracts approximately replicates the exchange-traded WPF contract. The EMC will thereby be able to hedge its volumetric risk by taking an appropriate position in the exchange-traded WPF, as in Eq. (5.5). A premium has to be paid from the individual WPP to the EMC in order to transfer the WPP's volumetric risk to the EMC. We return to this discussion in Sec. 5.2.3. However, the motivation for the EMC to engage in such tailor-made WPF contracts lies in this premium and the size of it compared to the premium in the exchange-traded WPF market. We mention in passing that to offset the potential residual volumetric risk of the portfolio described by Eq. (5.5), additional instruments could be added to the portfolio. This is outside the scope of present paper, and we leave this as future work.

5.2 Minimum variance hedge of a tailor-made WPF contracts portfolio

In this section we discuss a minimum variance hedge of a portfolio consisting of tailor-made WPF contracts for the EMC. I.e., from Eq. (5.5) we define the objective to

$$\min_{\gamma} \text{var}(R_C(\gamma)).$$

| Site ID | Capacity in MW, C_i | Price in EUR/MWh, Q_i |
|---------|-----------------------|-------------------------|
| 1 | 100 | 30 |
| 2 | 100 | 30 |
| 3 | 100 | 30 |

Table 5: Fictional contract specifications for the sites in Fig. 2.

The variance is

$$\begin{aligned}
\text{var}(R_C(\gamma)) &= \text{var} \left[\sum_{i=1}^{n-1} H \left(\frac{1}{T-S+1} \sum_{t=S}^T P_i(t) - P_i(t_0, S, T) \right) C_i Q_i \right. \\
&\quad \left. + \gamma H \left(\frac{1}{T-S+1} \sum_{t=S}^T P_n(t) - P_n(t_0, S, T) \right) X \right] \\
&= \sum_{i=1}^{n-1} \sum_{j=1}^{n-1} \left(\frac{H}{T-S+1} \right)^2 C_i Q_i C_j Q_j \sum_{t=S}^T \sum_{s=S}^T \text{cov}(P_i(t), P_j(s)) \\
&\quad + \left(\gamma \frac{H}{T-S+1} X \right)^2 \sum_{t=S}^T \sum_{s=S}^T \text{cov}(P_n(t), P_n(s)) \\
&\quad + 2 \sum_{i=1}^{n-1} \left(\frac{H}{T-S+1} \right)^2 \gamma X C_i Q_i \sum_{t=S}^T \sum_{s=S}^T \text{cov}(P_n(t), P_i(s)). \quad (5.6)
\end{aligned}$$

It follows from Eq. (5.6) that the optimal position of WPF contracts is

$$\gamma = - \frac{\sum_{i=1}^{n-1} C_i Q_i \sum_{t=S}^T \sum_{s=S}^T \text{cov}(P_n(t), P_i(s))}{X \sum_{t=S}^T \sum_{s=S}^T \text{cov}(P_n(t), P_n(s))}. \quad (5.7)$$

Besides the fact that the dependencies between the stochastic variables impact the size of γ , the size of each wind site measured by C_i and the price paid for each MWh to each wind site measured by Q_i both translate linearly to the size of γ . Therefore, the larger the wind site or the higher the price paid for each MWh, the larger γ will be in absolute terms (all other things being equal).

5.2.1 In-sample hedging effectiveness

In the following we consider the case of an EMC that needs to hedge its portfolio of tailor-made WPF from one year ahead to two years ahead. The considered wind sites are the ones depicted in Fig. 2. We assume that the contract specifications for each site is as shown in Table 5. Further, we assume that $X = 100$ EUR. The estimated parameters of the gamma and lognormal model are the ones reported in Sec. 4.

In Table 6 we present the hedging results for the gamma and lognormal model. We include the case with all three sites and the German WPF in the portfolio, and then three cases where we only include one of the wind sites and the German WPF. In each case, we report the model-implied optimal position of exchange-traded WPF contracts, $\hat{\gamma}$, and the variance reduction (in percentage) implied by the model calculated by $[\text{var}(R_C(0)) - \text{var}(R_C(\hat{\gamma}))]/\text{var}(R_C(0))$. It is apparent that the portfolio with all three sites outperforms the three other cases, confirming the diversification approach of the EMC discussed in Sec. 5.1.

| Case | Sites in portfolio | $\hat{\gamma}$ | $\text{var}(R_C(0))$ | $\text{var}(R_C(\hat{\gamma}))$ | Variance reduction (%) |
|-----------|--------------------|----------------|----------------------|---------------------------------|------------------------|
| Gamma | | | | | |
| 1 | 1,2,3 | -63.60 | $8.12 \cdot 10^{11}$ | $1.31 \cdot 10^{11}$ | 83.83 |
| 2 | 1 | -18.87 | $8.55 \cdot 10^{10}$ | $2.56 \cdot 10^{10}$ | 70.12 |
| 3 | 2 | -26.79 | $1.55 \cdot 10^{11}$ | $3.41 \cdot 10^{10}$ | 77.96 |
| 4 | 3 | -17.94 | $1.25 \cdot 10^{11}$ | $7.07 \cdot 10^{10}$ | 43.42 |
| Lognormal | | | | | |
| 1 | 1,2,3 | -64.00 | $7.06 \cdot 10^{11}$ | $1.21 \cdot 10^{11}$ | 82.89 |
| 2 | 1 | -18.97 | $8.12 \cdot 10^{10}$ | $2.98 \cdot 10^{10}$ | 63.33 |
| 3 | 2 | -25.10 | $1.34 \cdot 10^{11}$ | $4.42 \cdot 10^{10}$ | 67.04 |
| 4 | 3 | -19.92 | $1.13 \cdot 10^{11}$ | $5.66 \cdot 10^{10}$ | 50.05 |

Table 6: Optimal hedging quantity γ implied by the gamma and lognormal model for different portfolios consisting of different wind sites, and the corresponding variance of the portfolio excluding the exchange-traded WPF contract, and the variance of the portfolio when the optimal hedge is employed. Additionally, we show in all cases the associated variance reduction in percentage.

The fact that the difference regarding $\hat{\gamma}$ is small indicate that both models could be used interchangeably to determine an appropriate hedge, though the difference in variance reduction will mislead in a risk management context. In other words, if the wind indexes are driven by the gamma (lognormal) model, and one uses the lognormal (gamma) model to determine hedges, the variance reduction implied by the used model is wrong, while the hedging quantity is relatively close to the optimal hedge.

Comparing Eq. (5.4) to Eq. (5.5), the cases 2, 3, and 4 represent the variance reduction implied by the model if the individual wind sites were to hedge their power production themselves by using the exchange-traded WPF contract. From a social welfare point of view, the sum of variances of case 2, 3, and 4 is approximately 8% larger for both models compared to the variance of case 1. So not only does the model suggest that tailor-made WPF contracts constitute an obvious way of mitigating uncertainty for wind power producers, but also as a way of optimizing the integration of wind power penetration in the electricity grid from a total variance perspective.

5.2.2 Out-of-sample hedging effectiveness

In this section we consider the same portfolio of wind sites as in the previous case study, and the specifications of the sites are therefore specified in Table 5. However, here we assess the model on out-of-sample observations. We assume that an EMC has bought tailor-made WPF contracts at the three sites for the period from 2 July 2018 to 30 June 2019, corresponding to 364 days or 52 weeks. We employ a weekly minimum variance hedging strategy, meaning that the EMC has a naked position in a portfolio of tailor-made WPF contracts for the entire period with the exception of the front week. To concretize, the first position taken in exchange-traded WPF contracts is the contract with a weekly delivery period from 2 July 2018 to 8 July 2018. The position is taken based on a model that is estimated by using two years of observations ending the last trading day before the delivery period of the weekly exchange-traded WPF contract. With the delivery period starting the 2 July 2018, the last trading day

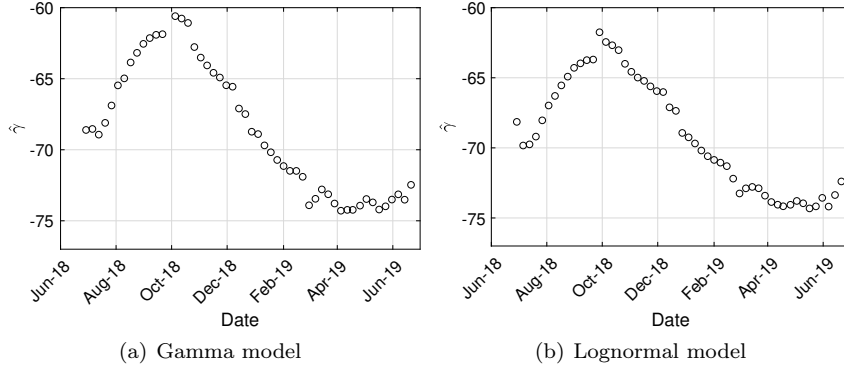


Figure 9: Variance minimizing hedge quantity, $\hat{\gamma}$, implied by (a) the gamma model and (b) the lognormal model for the 52 weeks covering the period from 2 July 2018 to 30 June 2019.

turns out to be 29 June 2018. Then we step one week ahead and determine the appropriate hedge for the week starting 9 July 2018 and ending 15 July 2018, but again only by employing two years of in-sample observations to estimate the model (the estimation period again ends on the last day where one can trade the weekly exchange-traded WPF contract). In this way we end up with 52 hedging quantities, where each quantity is calculated using different estimated parameters of the model due to the moving two-year observation period.

A comment on the model specifications is in place. The stationarity of the models in Sec. 3 might seem unreasonable in the present context, given the short period of time between an estimation date and the corresponding start date of delivery of the exchange-traded WPF contract. However, we also implemented the models that take the conditional distribution into account, resulting in similar results. For the sake of keeping the presentation as clear as possible, we have therefore only chosen to present the stationary versions of the models.

The resulting optimal hedge quantities are depicted in Fig. 9, indicating a seasonal pattern with more exchange-traded WPF contracts needed during spring compared to autumn. Considering Eq. (5.7), this is the result of the fact that the difference between the sum of the autocovariances of the German wind index and the sum of the autocovariances between the German wind index and the site indexes increases. To assess the hedging effectiveness, we calculate the corresponding implied weekly payoff, $R_C(\hat{\gamma})$, for each weekly hedge quantity, $\hat{\gamma}$. Since we have a variance minimizing perspective, we force a simplistic view on $P_i(t_0, S, T)$ for all wind indexes. Specifically, we assume that for each i , $P_i(t_0, S, T)$ for all weeks during the out-of-sample period from 2 July 2018 to 30 June 2019 is the mean of $P_i(t)$ over the first estimation period spanning 1 July 2016 to 29 June 2018,

Fig. 10 shows a histogram of the payoffs of the portfolio of tailor-made WPF contracts and the exchange-traded WPF contract acting as hedging instrument. Compared to Fig. 10(a), the variances in Fig. 10(b) and Fig. 10(c) are clearly reduced. In fact, the variance reduction in percentage of using the exchange-traded WPF contracts as hedging instrument is 93.64% for the gamma model

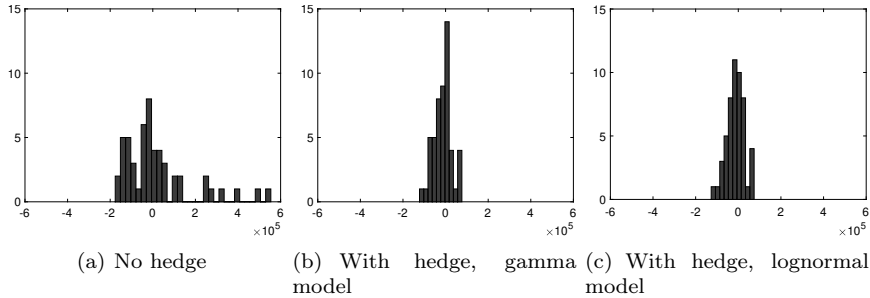


Figure 10: Histograms of (a) the payoff for EMC by not hedging the portfolio of tailor-made WPF contracts with exchange-traded WPF contracts, and (b)-(c) using the gamma and lognormal model to find the position in exchange-traded WPF contracts used as a hedging instrument for the portfolio of tailor-made WPF contracts.

and 93.62% for the lognormal model.

5.2.3 Risk premium of wind power futures

Since tailor-made WPF contracts are, by construction, traded over-the-counter, it is worth to discuss the risk premium of such contracts. As a reference point, we consider the risk premium of the exchange-traded WPF contracts. We define the risk premium as the model implied WPF contract price under the physical measure subtracted from the observed exchange-traded WPF contract price. The model implied price is defined by $\mathbb{E}[\bar{P}_n(S, T)]$, meaning that the risk premium $RP(t_0, S, T)$ is

$$RP(t_0, S, T) = \bar{P}_n(t_0, S, T) - \mathbb{E}[\bar{P}_n(S, T)] \quad (5.8)$$

on day t_0 for the delivery period $[S, T]$. The observed quoted exchange-traded WPF prices are obtained from NASDAQ OMX. As concluded in Sec. 5.2.2, the stationarity of the models does not imply different results compared to the conditional versions of the models for such long time periods, so to ease the presentation, we only consider the unconditional expected value here⁷.

We limit ourselves to yearly and quarterly exchange-traded WPF contracts for two reasons. First, it is unlikely that the tailor-made WPF contracts in general will be specified for a short delivery such as a week as a result of such non-standardized instrument. Secondly, as concluded in [6], fundamentals impact the information premium of exchange-traded WPF contracts with a short delivery period (e.g. a week) and a short period of time to delivery, which we would like to avoid. Thirdly, to assess the seasonal differences we also consider quarterly contracts.

For the period from 1 July 2016 to 30 June 2019, we show $\mathbb{E}[\bar{P}_n(S, T)]$ and $\bar{P}_n(t_0, S, T)$ in Fig. 11 for the front year (that is, for a given date, the front year denotes the next year). The quoted prices are fairly constant throughout the

⁷Despite the fact that $RP(t_0, S, T)$ still depends on t_0 through $\bar{P}_n(t_0, S, T)$, the assumption of stationarity is to some degree confirmed by the constant pattern of $\bar{P}_n(t_0, S, T)$ observed in Figs. 11 and 12(a).

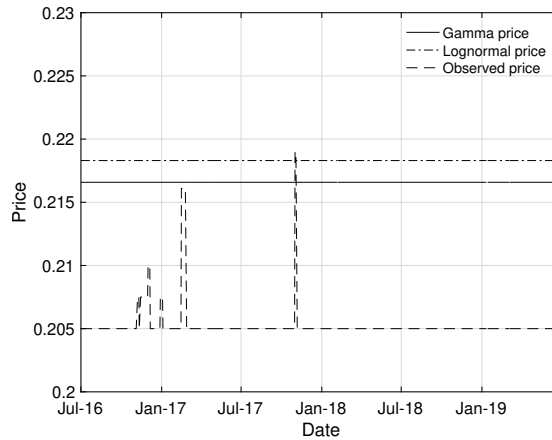


Figure 11: The model implied and quoted price for the front year for the period from 1 July 2016 to 30 June 2019. Notice that the date refers to the observation date; i.e., the date where the contract is quoted.

entire period, which could be a consequence of illiquidity of exchange-traded WPF contracts. The risk premium is -0.011 for the gamma model and -0.013 for the lognormal model on average. Since we are considering a yearly WPF contract we can ignore the seasonality and use the empirical mean to assess the risk premium. The empirical risk premium is -0.011 , agreeing with the gamma model. This is likely a consequence of the gamma model having a better fit to the distribution of the German wind index as discussed in Sec. 4 (see also Table 3).

Fig. 12(a) shows the model implied and quoted prices for the front quarter, and Fig. 12(b) shows the corresponding risk premium. The mean of the risk premium in this case is -0.014 for the gamma model and -0.016 for the lognormal model. The seasonal variation in the prices peaks for contracts with delivery during Q4 and Q1, simply since more wind is present during these quarters. This is also reflected in the model-implied prices. The peaks in the risk premium are observed for contracts with delivery during Q3 and Q24. One explanation of this could be non-aligned incentives to engage in the WPF market throughout the year for the buying and selling side. [9] shows that the hedging benefits are greater for CPPs during Q3 and Q4 compared to Q1 and Q2; hence, during Q3 and Q4, CPPs are more interested in WPF contracts and thus willing to pay more. In particular, this is observed for the contract with delivery during Q3 in 2017, where the risk premium even turns slightly positive for both models. We note that the observed spike for this contract, where the value of the risk premium becomes almost 0.03, corresponds to the trading activity on a single day.

A negative risk premium is in line with the findings in [6] and [10]. One might argue that this is expected from a hedging benefit perspective, since the hedging benefits in general are greater for the selling side than the buying side (see [8], [9], and [10]). Continuing this argument, the risk premium is likely to be even more negative in the tailor-made WPF market as a result of the perfect hedge implied by the tailor-made WPF contracts for WPPs. However,

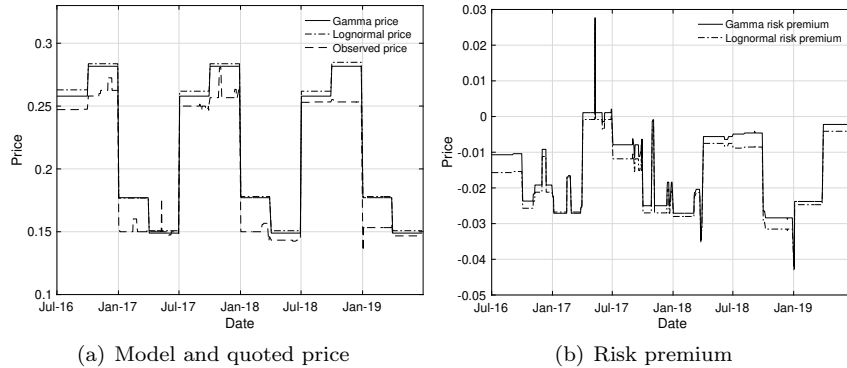


Figure 12: (a) the model implied and quoted price for the front quarter, and (b) the risk premium for the front quarter. The observations period is from 1 July 2016 to 30 June 2019. Notice that the date refers to the observation date; i.e., the date where the contract is quoted.

from the perspective of the individual WPP, this extra risk premium associated with the tailor-made WPF contract compared to the exchange-traded WPF contract has to be weighted against the deterministic payoff implied by the tailor-made WPF contract. Opposite, from the perspective of the EMC, this negative risk premium constitutes the motivation for engaging in the tailor-made WPF market and thereby taking over the volumetric risk.

6 Conclusion

In this paper, we propose and compare two multivariate continuous-time models, the gamma and lognormal model, for the joint behaviour of wind indexes. We discuss the properties of the models, and propose estimation procedures. Empirically, we employ the models to a joint model for the wind indexes at three different wind sites in Germany, and the German wind index that represents the overall utilization of wind power production in Germany. We find that both models are able to capture the autocorrelation structure well. However, the gamma model captures the skewness and kurtosis of the German wind index better than the lognormal model.

The models are applied to a variance-minimizing hedging strategy of a portfolio consisting of long positions in so-called tailor-made wind power futures contracts at the three wind sites, and a short position in the exchange-traded wind power futures contract. The hedging effectiveness is assessed in an in-sample and out-of-sample context. Both models indicate that a significant variance reduction can be obtained by hedging the portfolio with the exchange-traded wind power futures contracts in-sample as well as out-of-sample. Further, the hedging benefits are greater for the portfolio of tailor-made wind power futures compared to hedging each individual wind site with exchange-traded wind power futures contracts.

The risk premium of the exchange-traded wind power futures contracts is examined, where we find that the gamma model implies a more reliable estimate

of the risk premium. A negative risk premium is observed in line with other findings in the literature for both yearly and quarterly contracts. Even though the tailor-made wind power futures contracts give each wind power producer a perfect volumetric hedge of her wind power production, we argue that it is likely that the risk premium for a tailor-made wind power futures contract is even more negative compared to the exchange-traded contract.

Acknowledgements

Troels Sønderby Christensen is supported by the Innovation Fund Denmark under Grant 5189-00117B. Victor Rohde is supported by the Danish Council for Independent Research under Grant DFF-4002-00003.

A Theoretical results for the gamma model

This appendix is dedicated to proving Prop. 3.2 and Proposition 3.3. We start by proving Prop. 3.3, which the lemma below is a first step towards. We will use some standard results about continuous-time moving averages, all of which can be found in [14].

The following Lemma is well-known, but we give a proof for the sake of completeness.

Lemma A.1. *Let $t \geq 0$ and consider the two one-dimensional processes*

$$Y_1(t) = \int_{-\infty}^t f_1(t-u)dZ(u) \quad \text{and} \quad Y_2(t) = \int_{-\infty}^t f_2(t-u)dZ(u) \quad (\text{A.1})$$

for functions f_1 and f_2 in $L^1(\mathbb{R}) \cap L^2(\mathbb{R})$, and where Z is a one-dimensional Lévy process with second moment. Then

$$\mathbb{E}[Y_1(0)] = \int_0^\infty f_1(u)du\mathbb{E}[Z(1)]$$

and

$$\mathbb{E}[(Y_1(0) - \mathbb{E}[Y_1(0)])(Y_2(t) - \mathbb{E}[Y_2(t)])] = \int_0^\infty f_1(u)f_2(t+u)du \operatorname{var}(Z(1)).$$

Proof. Let $\psi_{Y_1(0), Y_2(t)}$ be the cumulant generating function of $(Y_1(0), Y_2(t))$ and ψ_Z be the cumulant generating function of Z . Then

$$\begin{aligned} \psi_{Y_1(0), Y_2(t)}(x) &= \log \mathbb{E}[\exp\{x_1 Y_1(0) + x_2 Y_2(t)\}] \\ &= \int_0^t \psi_Z(x_2 f_2(u))du + \int_0^\infty \psi_Z(x_1 f_1(u) + x_2 f_2(t+u))du. \end{aligned}$$

It follows that for $n_1, n_2 \in \mathbb{N}_0$ with $n_1 + n_2 \leq 2$,

$$\begin{aligned} \frac{d^{n_1+n_2}}{dx_1^{n_1} dx_2^{n_2}} \psi_{Y_1, Y_2}(x) &= \int_0^t f_2^{n_2}(u) \psi_Z^{(n_2)}(x_2 f_2(u))du \\ &\quad + \int_0^\infty f_1^{n_1}(u) f_2^{n_2}(u) \psi_Z^{(n_1+n_2)}(x_1 f_1(u) + x_2 f_2(u))du. \end{aligned}$$

where $\psi_Z^{(n_1+n_2)}$ denotes the $n_1 + n_2$ times derivative of ψ_Z . We conclude that

$$\mathbb{E}[Y_1(0)] = \frac{d}{dx_1} \psi_{Y_1(0), Y_2(t)}(0) = \int_0^\infty f_1(u) du \mathbb{E}[Z(1)].$$

Assume now, without loss of generality, $\mathbb{E}[Z(1)] = 0$. Then

$$\begin{aligned} & \mathbb{E}[(Y_1(0) - \mathbb{E}[Y_1(0)])(Y_2(t) - \mathbb{E}[Y_2(t)])] \\ &= \frac{d^2}{dx_1 dx_2} \psi_{Y_1(0), Y_2(t)}(0) \\ &= \int_0^\infty f_1(u) f_2(t+u) du \text{var}[Z(1)] \end{aligned}$$

□

Proof of Prop. 3.3. Let $\sigma_{i,k}$ denote the (i, k) 'th entry of Σ_L . Then, using Lemma A.1,

$$\begin{aligned} \mathbb{E}[X_i(t)] &= \sum_{k=1}^n \mathbb{E} \left[\int_{-\infty}^t e^{-\lambda_i(t-u)} \sigma_{i,k} dL_k(u) \right] \\ &= \sum_{k=1}^n \frac{1}{\lambda_i} \sigma_{i,k} \beta_k / 2 \\ &= (\Lambda^{-1} \Sigma_L \beta / 2)_i. \end{aligned}$$

This gives (3.9). Assume now, without loss of generality, $\mathbb{E}[L(1)] = 0$. Then, using Lemma A.1 again,

$$\begin{aligned} & \mathbb{E}[X_i(0) X_j(t)] \\ &= \mathbb{E} \left[\left(\sum_{k=1}^n \int_{-\infty}^0 e^{-\lambda_i(-u)} \sigma_{i,k} dL_k(u) \right) \left(\sum_{k=1}^n \int_{-\infty}^t e^{-\lambda_j(t-u)} \sigma_{j,k} dL_k(u) \right) \right] \\ &= \sum_{k=1}^n \sigma_{i,k} \sigma_{j,k} \int_0^\infty e^{-\lambda_j(t+u)} e^{-\lambda_i u} du \\ &= \frac{e^{-\lambda_j t}}{\lambda_i + \lambda_j} \sum_{k=1}^n \sigma_{i,k} \sigma_{j,k} \\ &= ((\Lambda_{var} \circ \Sigma_L \Sigma_L^\top) e^{-\Lambda t})_{i,j} \end{aligned}$$

from which (3.10) follows. □

We now turn to prove Prop. 3.2. Initially, we give the next result which is a special case of [7, Theorem 4.8], but again, we give a proof for the sake of completeness.

Proposition A.2. *Let L be a compound Poisson process with intensity $\alpha > 0$ and exponential jumps with parameter $\beta > 0$. Consider $t \in \mathbb{R}$, $\lambda, \mu > 0$ and $x_1, x_2 \in \mathbb{R}$ with $x_1 + x_2 < \beta$. Furthermore, assume $x_1 x_2 \geq 0$ and $x_1 \neq 0$, and*

let $f(t) = x_1 e^{-\lambda t} + x_2 e^{-\mu t}$. Then

$$\begin{aligned} & \log \mathbb{E} \left[\exp \left\{ \int_{-\infty}^t f(t-u) dL(u) \right\} \right] \\ &= \alpha \frac{f(0)}{f'(0)} \log \left(1 - \frac{f(0)}{\beta} \right) + \alpha \int_0^\infty \left(\frac{f(u)}{f'(u)} \right)' \log \left(1 - \frac{f(u)}{\beta} \right) du, \end{aligned} \quad (\text{A.2})$$

where

$$\left| \left(\frac{f(u)}{f'(u)} \right)' \right| \leq \frac{(\lambda - \mu)^2}{2\lambda\mu} \quad (\text{A.3})$$

for all $u \geq 0$.

Proof. Initially, note that f/f' is bounded and

$$\begin{aligned} \left| \left(\frac{f(u)}{f'(u)} \right)' \right| &= \frac{|f'(u)^2 - f(u)f''(u)|}{f'(u)^2} \\ &= \frac{x_1 x_2 (\lambda - \mu)^2 e^{-(\lambda+\mu)u}}{x_1^2 \lambda^2 e^{-2\lambda u} + x_2^2 \mu^2 e^{-2\mu u} + 2x_1 x_2 \lambda \mu e^{-(\lambda+\mu)u}} \\ &\leq \frac{(\lambda - \mu)^2}{2\lambda\mu}. \end{aligned}$$

This gives the bound on $(f/f)'$. Additionally, we find that

$$\begin{aligned} \left| \left(\frac{f(u)}{f'(u)} \right)' \right| &= \frac{x_1 x_2 (\lambda - \mu)^2 e^{-(\lambda+\mu)u}}{x_1^2 \lambda^2 e^{-2\lambda u} + x_2^2 \mu^2 e^{-2\mu u} + 2x_1 x_2 \lambda \mu e^{-(\lambda+\mu)u}} \\ &= \frac{x_1 x_2 (\lambda - \mu)^2}{x_1^2 \lambda^2 e^{-(\lambda-\mu)u} + x_2^2 \mu^2 e^{-(\mu-\lambda)u} + 2x_1 x_2 \lambda \mu}. \end{aligned}$$

We conclude that $(f(u)/f'(u))' = O(e^{-|\lambda-\mu|u})$ as $u \rightarrow \infty$. Thus, all integrals below are convergent and the integration by parts is justified. Next let

$$\psi(u) = \log \mathbb{E}[\exp(uL(1))] = \alpha \frac{u}{\beta - u}$$

be the cumulant-generating function of $L(1)$ and let $\phi(u) = -\alpha \log(1 - u/\beta)$ be the cumulant-generating function of a gamma distribution with shape α and rate β (see for example [6]). Note that $\psi(u) = u\phi'(u)$. Then, using integration by parts,

$$\begin{aligned} & \log \mathbb{E} \left[\exp \left\{ \int_{-\infty}^t f(t-u) dL(u) \right\} \right] \\ &= \int_0^\infty \psi(f(u)) du \\ &= \int_0^\infty \frac{f(u)}{f'(u)} (\phi(f(u)))' du \\ &= -\frac{f(0)}{f'(0)} \phi(f(0)) - \int_0^\infty \left(\frac{f(u)}{f'(u)} \right)' \phi(f(u)) du. \end{aligned}$$

□

Remark A.3. Considering the proof of Prop. A.2 there are two approaches to calculate

$$\log \mathbb{E} \left[\exp \left\{ \int_{-\infty}^t f(t-u) dL(u) \right\} \right]. \quad (\text{A.4})$$

Either by calculating

$$\int_0^{\infty} \psi(f(u)) du \quad (\text{A.5})$$

or

$$-\frac{f(0)}{f'(0)} \phi(f(0)) - \int_0^{\infty} \left(\frac{f(u)}{f'(u)} \right)' \phi(f(u)) du. \quad (\text{A.6})$$

Here, ψ and ϕ are the cumulant-generating function of $L(1)$ and of a gamma distribution with shape α and rate β as defined in the proof of Prop. A.2. By (A.3), the integral in (A.6) will be small whenever $(\lambda - \mu)^2 / (2\lambda\mu)$ is small. In the application we consider we are concerned with the case where $\lambda = \hat{\lambda}_i$ and $\mu = \hat{\lambda}_j$ for some $i, j = 1, 2, 3, 4$, where $\hat{\lambda}_i$ and $\hat{\lambda}_j$ are given in Table 2. We have

$$\max_{i,j} \frac{(\hat{\lambda}_i - \hat{\lambda}_j)^2}{2\hat{\lambda}_i\hat{\lambda}_j} = 0.0506,$$

and therefore, indeed, that $(\lambda - \mu)^2 / (2\lambda\mu)$ is small in the case relevant to us. The integral in (A.6) has ϕ in the kernel whereas (A.5) has ψ , making a direct comparison more difficult. We do, however, have

$$\phi(u) = \alpha u + O(u^2) \text{ and } \psi(u) = \alpha u + O(u^2) \text{ as } u \rightarrow 0$$

(by a Taylor approximation argument), indicating that ϕ and ψ are of comparable size, at least for small values. Furthermore, by numerical comparison, we have found them to be of similar size. We conclude that the kernel of (A.6) is expected to be considerably smaller than the kernel of (A.5). We therefore prefer to do the calculation in (A.6) instead of (A.5) since we can do a much more coarse approximation for a desired precision of an approximation of (A.4).

Proposition A.4. *Let L be a compound Poisson process with intensity $\alpha > 0$ and exponential jumps with parameter $\beta > 0$. Consider $s < t$, $\lambda > 0$ and $x < \beta$. Then*

$$\mathbb{E} \left[\exp \left\{ x \int_s^t e^{-\lambda(t-u)} dL(u) \right\} \right] = \left(\frac{\beta - x e^{-\lambda(t-s)}}{\beta - x} \right)^{\alpha/\lambda}$$

and

$$\mathbb{E} \left[\exp \left\{ x \int_{-\infty}^t e^{-\lambda(t-u)} dL(u) \right\} \right] = \left(\frac{\beta}{\beta - x} \right)^{\alpha/\lambda} \quad (\text{A.7})$$

Proof. Let

$$\psi(t) = \log \mathbb{E}[\exp(tL(1))] = \alpha \frac{t}{\beta - t}$$

be the cumulant-generating function of L . Then

$$\begin{aligned} & \log \mathbb{E} \left[\exp \left\{ \int_s^t f(t-u) dL(u) \right\} \right] \\ &= \int_0^{t-s} \psi(e^{-\lambda u}) du \\ &= \frac{\alpha}{\lambda} \left(\log(\beta - x e^{-\lambda(t-s)}) - \log(\beta - x) \right). \end{aligned}$$

A similar calculation gives (A.7). \square

Proof of Theorem 3.2. For notional convenience, let

$$\tilde{L}(t) = (L_1(t), \dots, L_{n-1}(t), 0, L_n(t))^\top \in \mathbb{R}^{n+1}.$$

First consider (3.7) and assume $i \neq j$. We have

$$\begin{aligned} X_i(t) &= \int_{-\infty}^t e^{-\lambda_i(t-u)} \tilde{\sigma}_{i,i} d\tilde{L}_i(u) + \int_s^t e^{-\lambda_i(t-u)} \tilde{\sigma}_{i,n+1} d\tilde{L}_{n+1}(u) \\ &+ \int_{-\infty}^s e^{-\lambda_i(t-u)} \tilde{\sigma}_{i,n+1} d\tilde{L}_{n+1}(u) \end{aligned}$$

and

$$X_j(s) = \int_{-\infty}^s e^{-\lambda_j(s-u)} \tilde{\sigma}_{j,j} d\tilde{L}_j(u) + \int_{-\infty}^s e^{-\lambda_j(s-u)} \tilde{\sigma}_{j,n+1} d\tilde{L}_{n+1}(u).$$

Next, note that $\text{cov}(UV, W) = \text{cov}(V, UW) = \mathbb{E}[U] \text{cov}(V, W)$ for a random variable U independent of the random variables V and W . Applying this, and the above, we conclude that

$$\begin{aligned} & \text{cov}(P_i(t), P_j(s)) \\ &= \text{cov} \left(e^{-S_i(t)} X_i(t), e^{-S_j(s)} X_j(s) \right) \\ &= \mathbb{E} \left[\exp \left\{ -S_i(t) \int_{-\infty}^t e^{-\lambda_i(t-u)} \tilde{\sigma}_{i,i} d\tilde{L}_i(u) \right\} \right] \\ & \times \mathbb{E} \left[\exp \left\{ -S_i(t) \int_s^t e^{-\lambda_i(t-u)} \tilde{\sigma}_{i,n+1} d\tilde{L}_{n+1}(u) \right\} \right] \\ & \times \mathbb{E} \left[\exp \left\{ -S_j(s) \int_{-\infty}^s e^{-\lambda_j(s-u)} \tilde{\sigma}_{j,j} d\tilde{L}_j(u) \right\} \right] \\ & \times \text{cov} \left(\exp \left\{ -S_i(t) \int_{-\infty}^s e^{-\lambda_i(t-u)} \tilde{\sigma}_{i,n+1} d\tilde{L}_i(u) \right\}, \right. \\ & \quad \left. \exp \left\{ -S_j(s) \int_{-\infty}^s e^{-\lambda_j(s-u)} \tilde{\sigma}_{j,n+1} d\tilde{L}_{n+1}(u) \right\} \right) \end{aligned} \tag{A.8}$$

Expressions of the three expectations in Eq. (A.8) are given in Prop. A.4. Fur-

thermore,

$$\begin{aligned}
& \text{cov} \left(\exp \left\{ -S_i(t) \int_{-\infty}^s e^{-\lambda_i(t-u)} \tilde{\sigma}_{i,n+1} d\tilde{L}_i(u) \right\}, \right. \\
& \quad \left. \exp \left\{ -S_j(s) \int_{-\infty}^s e^{-\lambda_j(s-u)} \tilde{\sigma}_{j,n+1} d\tilde{L}_{n+1}(u) \right\} \right) \\
&= \mathbb{E} \left[\exp \left\{ - \int_{-\infty}^s f_{i,j}(s-u) d\tilde{L}_{n+1}(u) \right\} \right] \\
& \quad - \mathbb{E} \left[\exp \left\{ -S_i(t) \int_{-\infty}^s e^{-\lambda_i(t-u)} \tilde{\sigma}_{i,n+1} d\tilde{L}_{n+1}(u) \right\} \right] \\
& \quad \times \mathbb{E} \left[\exp \left\{ -S_j(s) \int_{-\infty}^s e^{-\lambda_j(s-u)} \tilde{\sigma}_{j,n+1} d\tilde{L}_{n+1}(u) \right\} \right]
\end{aligned}$$

for which expressions are given in Prop. A.2 and Prop. A.4.

Next, consider (3.8). We write

$$\begin{aligned}
X_i(t) &= \int_s^t e^{-\lambda_i(t-u)} \left(\tilde{\sigma}_{i,i} d\tilde{L}_i(u) + \tilde{\sigma}_{i,n+1} d\tilde{L}_{n+1}(u) \right) \\
& \quad + \int_{-\infty}^s e^{-\lambda_i(t-u)} \left(\tilde{\sigma}_{i,i} d\tilde{L}_i(u) + \tilde{\sigma}_{i,n+1} d\tilde{L}_{n+1}(u) \right)
\end{aligned}$$

and

$$X_i(s) = \int_{-\infty}^s e^{-\lambda_i(s-u)} \left(\tilde{\sigma}_{i,i} d\tilde{L}_i(u) + \tilde{\sigma}_{i,n+1} d\tilde{L}_{n+1}(u) \right).$$

Consequently,

$$\begin{aligned}
& \text{cov}(P_i(t), P_i(s)) \\
&= \text{cov} \left(e^{-S_i(t)X_i(t)}, e^{-S_i(s)X_i(s)} \right) \\
&= \mathbb{E} \left[\exp \left\{ -S_i(t) \int_s^t e^{-\lambda_i(t-u)} \left(\tilde{\sigma}_{i,i} d\tilde{L}_i(u) + \tilde{\sigma}_{i,n+1} d\tilde{L}_{n+1}(u) \right) \right\} \right] \\
& \quad \times \text{cov} \left(\exp \left\{ -S_i(t) \int_{-\infty}^s e^{-\lambda_i(t-u)} \left(\tilde{\sigma}_{i,i} d\tilde{L}_i(u) + \tilde{\sigma}_{i,n+1} d\tilde{L}_{n+1}(u) \right) \right\}, \right. \\
& \quad \left. \exp \left\{ -S_i(s) \int_{-\infty}^s e^{-\lambda_i(s-u)} \left(\tilde{\sigma}_{i,i} d\tilde{L}_i(u) + \tilde{\sigma}_{i,n+1} d\tilde{L}_{n+1}(u) \right) \right\} \right)
\end{aligned}$$

Again, expressions for the expectation in (A.8) can be found using Prop. A.4.

Finally,

$$\begin{aligned}
& \text{cov} \left(\exp \left\{ -S_i(t) \int_{-\infty}^s e^{-\lambda_i(t-u)} \left(\tilde{\sigma}_{i,i} d\tilde{L}_i(u) + \tilde{\sigma}_{i,n+1} d\tilde{L}_{n+1}(u) \right) \right\}, \right. \\
& \quad \left. \exp \left\{ -S_i(s) \int_{-\infty}^s e^{-\lambda_i(s-u)} \left(\tilde{\sigma}_{i,i} d\tilde{L}_i(u) + \tilde{\sigma}_{i,n+1} d\tilde{L}_{n+1}(u) \right) \right\} \right) \\
&= \mathbb{E} \left[\exp \left\{ - \int_{-\infty}^s \tilde{\sigma}_{i,i} \left(S_i(t) e^{-\lambda_i(t-s)} + S_i(s) \right) e^{-\lambda_i(s-u)} d\tilde{L}_i(u) \right\} \right] \\
& \quad \times \mathbb{E} \left[\exp \left\{ - \int_{-\infty}^s \tilde{\sigma}_{i,n+1} \left(S_i(t) e^{-\lambda_i(t-s)} + S_i(s) \right) e^{-\lambda_i(s-u)} d\tilde{L}_{n+1}(u) \right\} \right] \\
&= \mathbb{E} \left[\exp \left\{ - \int_{-\infty}^s \tilde{\sigma}_{i,i} S_i(t) e^{-\lambda_i(t-u)} d\tilde{L}_i(u) \right\} \right] \\
& \quad \times \mathbb{E} \left[\exp \left\{ - \int_{-\infty}^s \tilde{\sigma}_{i,n+1} S_i(t) e^{-\lambda_i(t-u)} d\tilde{L}_{n+1}(u) \right\} \right] \\
& \quad \times \mathbb{E} \left[\exp \left\{ - \int_{-\infty}^s \tilde{\sigma}_{i,i} S_i(s) e^{-\lambda_i(s-u)} d\tilde{L}_i(u) \right\} \right] \\
& \quad \times \mathbb{E} \left[\exp \left\{ - \int_{-\infty}^s \tilde{\sigma}_{i,n+1} S_i(s) e^{-\lambda_i(s-u)} d\tilde{L}_{n+1}(u) \right\} \right]
\end{aligned}$$

whose expressions are given in Prop. A.4. □

References

- [1] Asmussen, S., Jensen, J. L., Rojas-Nandayapa, L. (2016). On the Laplace transform of the lognormal distribution. *Methodology and Computing in Applied Probability*, **18**, pp. 441–458.
- [2] Ballotta, L., Bonfiglioli, E. (2016). Multivariate asset models using Lévy processes and applications. *The European Journal of Finance*, **22(13)**, pp. 1320–1350.
- [3] Barndorff-Nielsen, O. E., Shephard, N. (2001). Non-Gaussian Ornstein–Uhlenbeck-based models and some of their uses in financial economics. *Journal of the Royal Statistical Society: Series B (Statistical Methodology)*, **63(2)**, pp. 167–241.
- [4] Benth, F. E., Benth, J. Š. (2007). The volatility of temperature and pricing of weather derivatives. *Quantitative Finance*, **7(5)**, pp. 553–561.
- [5] Benth, F. E., Kallsen, J., Meyer-Brandis, T. (2007). A non-Gaussian Ornstein–Uhlenbeck process for electricity spot price modeling and derivatives pricing. *Applied Mathematical Finance*, **14(2)**, pp. 153–169.
- [6] Benth, F. E., Pircalabu, A. (2018). A non-Gaussian Ornstein–Uhlenbeck model for pricing wind power futures. *Applied Mathematical Finance*, **25**, pp. 36–65.
- [7] Benth, F. E., Rohde, V. (2019). On non-negative modeling with CARMA processes. *Journal of Mathematical Analysis and Applications*, **476(1)**, pp. 196–214.
- [8] Christensen, T. S., Pircalabu, A. (2018). On the spatial hedging effectiveness of German wind power futures for wind power generators. *Journal of Energy Markets*, **11**, pp. 71–96.
- [9] Christensen, T. S., Pircalabu, A., Høg, E. (2019). A seasonal copula mixture for hedging the clean spark spread with wind power futures *Energy Economics*, **78**, pp. 64–80.
- [10] Gersema, G. and Wozabal, D. (2017). An equilibrium pricing model for wind power futures. *Energy Economics*, **65**, pp. 64–74.
- [11] Halliwell, L. J. (2015). The lognormal random multivariate. *Casualty Actuarial Society E-Forum*.
- [12] Leoni, P., Schoutens, W. (2008). Multivariate Smiling. *Wilmott Magazines*.
- [13] Meucci, A. (2009). Review of statistical arbitrage, cointegration, and multivariate Ornstein-Uhlenbeck. Available at SSRN: <https://ssrn.com/abstract=1404905>.
- [14] Rajput, B. S., Rosinski, J. (1989). Spectral representations of infinitely divisible processes. *Probability Theory and Related Fields*, **82(3)**, pp. 451–487.

- [15] Sato, K. I. (1999). Lévy processes and infinitely divisible distributions. *Cambridge University Press*.
- [16] Semeraro, P. (2008). A multivariate variance gamma model for financial application. *International Journal of Theoretical and Applied Finance*, **11(1)**, pp. 1–18.